J Appl Electrochem (2012) 42:893–899
DOI 10.1007/s10800-012-0472-7

ORIGINAL PAPER

Soft magnetic properties of Ni–Cr and Co–Cr alloy thin films electrodeposited from aqueous solutions containing trivalent chromium ions and glycine

T. Ohgai · Y. Tanaka · T. Fujimaru

Received: 27 May 2012 / Accepted: 10 August 2012 / Published online: 18 August 2012

Abstract Ferromagnetic Ni–Cr and Co–Cr alloy thin films were electrodeposited from aqueous solution containing trivalent chromium (Cr^{3+}) ions and glycine. According to the Tafel slopes obtained from the cathode polarization curves for Ni–Cr and Co–Cr alloy deposition, it was estimated that Cr^{3+} ions inhibited Ni^{2+} and Co^{2+} ions from electrodepositing. Ni and Co preferentially electrodeposited rather than Cr and the electrodeposition process of Ni–Cr and Co–Cr was categorized to "normal co-deposition type." At the cathode potential of −1.8 V versus Ag/AgCl/KCl sat., Ni—9.5 %Cr and Co—8.4 %Cr alloy deposits were obtained. X-ray diffraction patterns of the electrodeposits revealed that pure Ni and pure Co consist of large crystal grains, while Ni—9.5 %Cr and Co—8.4 %Cr alloys were composed of a solid solution phase with fine crystal grains. Magnetization of Ni—9.5 %Cr and Co—8.4 %Cr alloy thin films with fine crystalline phase reached to saturation at ca. 2.5 kOe in perpendicular direction to the film plane, while pure Ni and pure Co thin film with large crystal grains were hardly magnetized in the perpendicular direction. Soft magnetic properties were improved with increasing Cr content in the deposits.

T. Ohgai (✉) · T. Fujimaru
Department of Materials Science and Engineering, Nagasaki University, 1-14, Bunkyo-machi, Nagasaki 852-8521, Japan
e-mail: ohgai@nagasaki-u.ac.jp

Y. Tanaka
TDK Corporation, 2-15-7 Higashi-Ohwada, Ichikawa-shi, Chiba 272-8558, Japan

T. Fujimaru
Hiroshima Machinery Works, Mitsubishi Heavy Industries Ltd., 4-6-22, Kan-on-shin-machi, Nishi-ku, Hiroshima 733-8553, Japan

Keywords Magnetic property · Electrodeposition · Trivalent chromium ions · Nickel · Cobalt

1 Introduction

Chromium (Cr) has a high melting point (T_m) of 2,136 K and is chemically stable under various conditions. Therefore, Cr can be applied to an alloying element for high temperature super alloys (Hastelloy, Inconel, etc.), jet engines, gas turbines, high speed steels, stainless steels, and high corrosion resistance alloys. Usually, Cr alloys are produced by a pyrometallurgical process under the condition of high temperature and vacuum in a closed chamber. However, it is quite difficult to obtain Cr alloys at room temperature due to the high T_m and mechanical hardness. On the contrary, in a conventional electroplating process, metallic Cr films can be synthesized by electrodeposition from an aqueous solution containing hexavalant chromium ions (Cr^{6+}) under the condition of room temperature and atmospheric pressure [1–3]. However, Cr^{6+} ions are known to toxic and carcinogenic substances; hence, in recent years, the solution containing trivalent chromium ions (Cr^{3+}) have been applied to an electrolyte for Cr electroplating instead of the solution containing Cr^{6+} ions [4, 5]. Current efficiency for Cr deposition from the solution containing Cr^{3+} ions is lower than that of the other transition metals such as Fe, Co, Ni, Cu, Zn, etc., and is up to ca. 20–30 %. Therefore, the organic compounds such as formic acid [6], acetic acid [7], citric acid [8], glycolic acid [8], oxalic acid [9], etc., have been investigated as a complexing agent for Cr^{3+} ions to improve the current efficiency for Cr deposition. Furthermore, N-containing compounds, such as glycine [10], urea [11–13], thiocyanate [14], etc., have been also investigated to improve the surface appearance of Cr deposits. Nitrogen atoms in N-containing

Table 1 Bath compositions for electrodeposition of Ni, Ni–Cr, Co, and Co–Cr alloys

Electrolyte (mol/L)	Ni	Ni–Cr	Co	Co–Cr
$[CrCl_3{\cdot}6H_2O]$	–	0.9	–	0.9
$[NiCl_2{\cdot}6H_2O]$	0.1	0.1	–	–
$[CoCl_2{\cdot}6H_2O]$	–	–	0.1	0.1
$[H_3BO_3]$	0.7	0.7	0.7	0.7
$[H_2NCH_2COOH]$	1.0	1.0	1.0	1.0
$[HCOONH_4]$	1.8	1.8	1.8	1.8
R_{Cr}^{Bath} (%)	0	90	0	90

compounds have lone pairs of electrons which can act as catalysts to promote the electrochemical charge transfer reaction on a cathode.

Electrodeposited iron-group metal alloys containing Cr (M–Cr alloys) consist of a nanocrystalline phase or an amorphous phase [15]. Harris et al. [16] reported that the ternary Ni–Fe–Cr alloys containing 8 %Cr was electrodeposited from an aqueous solution containing acetic acid. They found that the acetic acid served to limit the precipitation of nonmetallic material on the electrode by forming a soluble complex with Cr^{3+} ions. Kang et al. [6] reported that the amorphous Fe–Ni–Cr alloys were electrodeposited from an aqueous solution containing formic acid and hypophosphite. They found that the phosphorus and carbon in the alloy deposits improved the Knoop hardness value.

Nanocrystalline or amorphous iron-group metal alloys are known for showing the excellent soft magnetic properties [17] which can be applied to high sensitive magnetic field sensors with high corrosion resistance. For example, magnetic field sensors with corrosion resistance can be equipped to monitor the wheel rotation rate in antilock brake system (ABS) for automobiles [18]. However, few research works have been reported on the magnetic properties of electrodeposited M–Cr alloys. Hence, the effect of N-containing compounds on the nanocrystalline structure and the soft magnetic properties in electrodeposited M–Cr alloys is still in an unsettled issue. In this study, Ni–Cr and Co–Cr alloy thin films were electrodeposited from an aqueous solution containing Cr^{3+} ions and glycine as a N-containing complexing agent to investigate the formation of a nanocrystalline phase and the magnetization behavior.

2 Experimental

Bath compositions for the electrodeposition of Ni–Cr and Co–Cr alloys are shown in Table 1. The electrolytic solutions were synthesized from $NiCl_2{\cdot}6H_2O$ ($CoCl_2{\cdot}6H_2O$), $CrCl_3{\cdot}6H_2O$, H_3BO_3, H_2NCH_2COOH (glycine), and $HCOONH_4$ (ammonium formiate). Here, Cr^{3+} ion concentration ratio in bath $\{R_{Cr}^{bath} = 100 \times [Cr^{3+}]/([Cr^{3+}] + [Ni^{2+} \text{ or } Co^{2+}])\}$ was adjusted to 90 % and the solution pH was kept to 4.0. Copper foils with a thickness of 30 μm were used as cathodes for electrodepositing Ni–Cr and Co–Cr alloy thin films. A platinum wire and Ag/AgCl/KCl sat. electrodes were used as an anode and a reference electrode. To determine the optimum cathode potential range for electrodepositing Ni–Cr and Co–Cr alloys, cathode polarization curves were measured over the wide potential range from 0 to −2.0 V. Ni–Cr and Co–Cr alloy thin films with the thickness of ca. 1 μm were electrodeposited potentiostatically at 303 K.

To investigate the relationship between the cathode potential during the electrodeposition and Cr content in the deposits $\{R_{Cr}^{depo} = 100 \times [Cr]/([Cr] + [Ni \text{ or } Co])\}$, composition of the electrodeposits was determined by an energy dispersive X-ray spectrometry (EDX). Constituent phase, crystallinity, and the surface morphology of electrodeposited Ni–Cr and Co–Cr alloy thin films were evaluated by X-ray diffraction (XRD) and scanning electron microscopy (SEM). Magnetization behavior of electrodeposited Ni–Cr and Co–Cr alloy thin films with Cu foils was investigated using a vibrating sample magnetometer (VSM) with increasing the magnetic field up to 10 kOe. Magnetic field was applied to inplane and perpendicular direction to the film plane.

3 Results and discussion

3.1 Electrodeposition process of Ni–Cr and Co–Cr alloys

Figure 1 shows the effect of Cr^{3+} ions on the cathode polarization curves for pure Ni and Ni–Cr alloy deposition. The cathode current begins to occur at ca. −0.2 to −0.3 V, which is more-noble than the equilibrium potential of Ni^{2+}/Ni ($E_{Ni}^{eq} = -0.46$ V vs. Ag/AgCl/KCl sat.) and Cr^{3+}/Cr ($E_{Cr}^{eq} = -0.93$ V). Therefore, this cathode current is mainly caused by the reduction of hydrogen ions (H^+). With increasing the cathode current density (CCD), at around 5 A m^{-2}, the potential polarizes to be around −0.7 V due to the diffusion limit of H^+ ions. At around −0.7 V, the CCD increases again. This increase in CCD is mainly caused by the electrodeposition of pure Ni or Ni–Cr alloys. In this CCD region, charge transfer process will control the electrochemical reaction rate and the relationship between the overpotential (η) and CCD (i) can be expressed by the following Tafel equation:

$$\eta = a + b \log i \quad (1)$$

Tafel slopes (b) estimated from the cathode polarization curves for pure Ni and Ni–Cr alloy deposition are ca. 0.06 V (b_{Ni}) and 0.14 V (b_{Ni-Cr}) as shown in Fig. 1. The charge transfer coefficient (α) can be estimated by the following equation using Tafel slope (b):

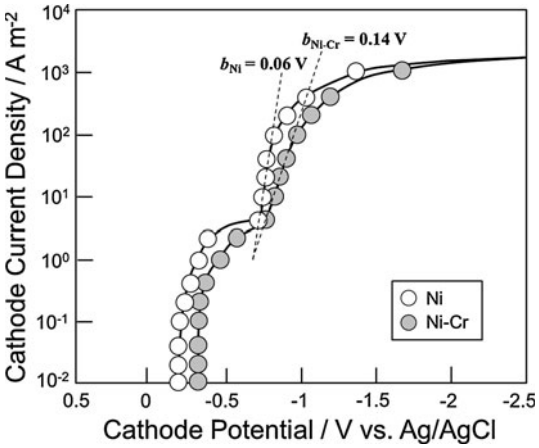

Fig. 1 Effect of Cr^{3+} ions on the cathode polarization curves for pure Ni and Ni–Cr alloy deposition

$$\alpha = 2.303RT/(nFb) \quad (2)$$

Here, R, T, n, and F are the gas constant, the absolute temperature, the number of electrons involved in the electrode reaction, and the Faraday constant, respectively. The charge transfer coefficient (α) calculated from b_{Ni} and b_{Ni-Cr} are ca. 0.52 (α_{Ni}) and 0.21 (α_{Ni-Cr}), respectively. Therefore, it is estimated that Cr^{3+} ions inhibited Ni^{2+} ions from electrodepositing.

Effect of Cr^{3+} ions on the cathode polarization curves for pure Co and Co–Cr alloy deposition was shown in Fig. 2. The cathode current begins to occur at ca. −0.2 to −0.3 V, which is more-noble than the equilibrium potential of Co^{2+}/Co ($E^{eq}_{Co} = -0.50$ V) and Cr^{3+}/Cr ($E^{eq}_{Cr} = -0.93$ V). Therefore, this cathode current is mainly caused by the reduction of hydrogen ions (H^+). Similar tendency was observed in the electrodeposition behavior of Ni–Cr alloys and Co–Cr alloys as shown in Figs. 1 and 2. Tafel slopes (b) estimated from the cathode polarization curves for pure Co and Co–Cr alloy deposition are ca. 0.06 V (b_{Co}) and 0.16 V (b_{Co-Cr}) as shown in Fig. 2. The charge transfer coefficient (α) calculated from b_{Co} and b_{Co-Cr} are ca. 0.52 (α_{Co}) and 0.19 (α_{Co-Cr}). Hence, it is also estimated that Cr^{3+} ions inhibited Co^{2+} ions from electrodepositing. At the potential region less than −2.0 V with increasing CCD the potential polarizes significantly to be less-noble region due to the diffusion limit of Ni^{2+} and Cr^{3+} ions. It is well known that the morphology of electrodeposits has changed from an ideal smooth surface to a powder-like rough deposit with increase in CCD up to the diffusion limit of metal ions. Consequently, the optimum cathode potential range for electrodeposition of Ni–Cr and Co–Cr alloys is determined to be from −1.1 to −1.8 V.

Figure 3 shows the effect of cathode potential on Cr content in Ni–Cr and Co–Cr alloy deposits. With increase in cathode potential to less-noble direction, Cr content in the deposits also increases and Ni and Co preferentially electrodeposited rather than Cr. For example, Ni—9.5 %Cr alloy deposit ($R^{depo}_{Cr} = 9.5$ %) was obtained from the solution containing 90 % of Cr^{3+} ($R^{bath}_{Cr} = 90$ %). In this condition, R^{depo}_{Cr} was diluted ca. 0.1 times lower than R^{bath}_{Cr}. In the same way, Co—8.4 %Cr alloy deposit ($R^{depo}_{Cr} = 8.4$ %) was obtained from the solution containing 90 % of Cr^{3+} ($R^{bath}_{Cr} = 90$ %). In this condition, R^{depo}_{Cr} was also diluted ca. 0.09 times lower than R^{bath}_{Cr}. It is well known that in the binary (A–B) alloy electrodeposition process if there is no interaction between A and B; electrochemically noble metal will electrodeposit preferentially. This co-deposition process can be categorized to "normal co-deposition type" according to Brenner's classification [19]. Dolati et al. [8] reported that the quaternary Fe–Cr–Ni–Mo alloys was electrodeposited from an aqueous solution containing citric acid and glycolic acid. According to their report, $Fe_{66}Cr_{19}Ni_{13}Mo_2$ alloys ($R^{depo}_{Cr} = 19$ %) was obtained from the solution containing ca. 80 % of Cr^{3+} ($R^{bath}_{Cr} = 80$ %) and iron-group metals such as Fe and Ni deposited preferentially

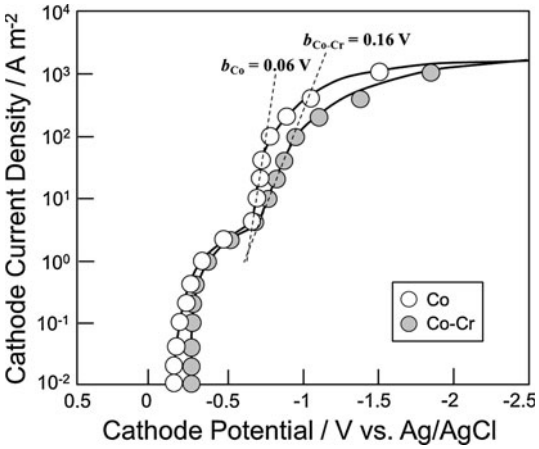

Fig. 2 Effect of Cr^{3+} ions on the cathode polarization curves for pure Co and Co–Cr alloy deposition

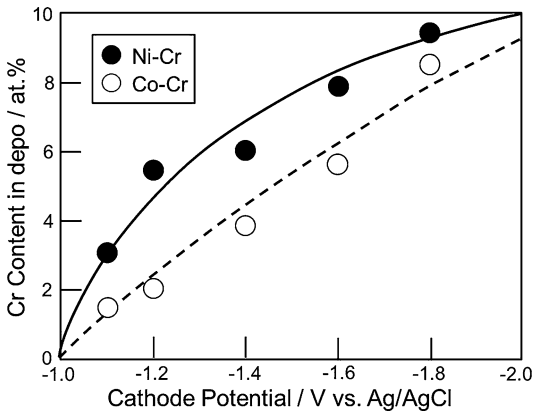

Fig. 3 Effect of cathode potential on Cr content in Ni–Cr and Co–Cr alloy deposits

rather than the less-noble Cr from an aqueous solution. Therefore, in the present work, the co-deposition process of Ni–Cr and Co–Cr can be also categorized to "normal co-deposition type." R_{Cr}^{depo} in Ni–Cr alloy deposits was larger than that in Co–Cr alloy deposits as shown in Fig. 3. According to the phase diagram [20], the solubility limit of Cr in Ni–Cr alloy is ca. 23 %, while that in Co–Cr alloy is ca. 14 %. Therefore, the difference of co-deposition behavior in Ni–Cr and Co–Cr alloys would be caused by the difference of solubility limit of Cr in the alloys.

3.2 Structure of electrodeposited Ni–Cr and Co–Cr alloys

Figure 4 shows the X-ray diffraction profiles obtained from electrodeposited pure Ni, Ni—5.6 %Cr, Ni—6.0 %Cr, and Ni—9.5 %Cr alloys. In the diffraction profile obtained from electrodeposited pure Ni, most close-packed crystal plane Ni (111) and Ni (200) were observed as main peaks and the diffraction peaks shifted to the lower 2θ region with increasing R_{Cr}^{depo}. This is resulting from the formation of a solid solution α phase in the electrodeposited Ni–Cr alloys. On the contrary, intensity of α (111) and α (200) was decreased and the shape of peaks has changed to be broad with increasing R_{Cr}^{depo}. Figure 5 shows the X-ray diffraction profiles obtained from electrodeposited pure Co, Co—2.0 %Cr, Co—3.8 %Cr, and Co—8.4 %Cr alloys. In the diffraction profile obtained from electrodeposited pure Co, hcp-Co (100) was observed as main peak and the diffraction peak shifted to the lower 2θ region with increasing R_{Cr}^{depo}. This is resulting from the formation of a solid solution ε phase in the electrodeposited Co–Cr alloys. On the contrary, intensity of ε (100) was decreased and the shape of peaks has changed to be broad with increasing R_{Cr}^{depo}. These results suggest that the electrodeposited Ni–Cr and Co–Cr alloys would be composed of a fine-crystalline phase or an amorphous phase [6, 15].

According to the phase diagram of Ni–Cr binary alloy system [20], the solubility limit of Cr in α phase is ca. 23 %

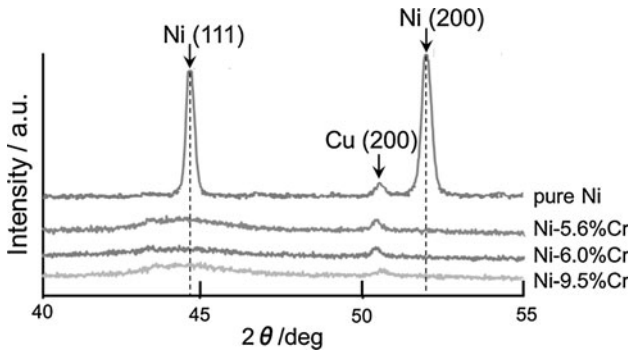

Fig. 4 X-ray diffraction profiles obtained from electrodeposited pure Ni, Ni—5.6 %Cr, Ni—6.0 %Cr, and Ni—9.5 %Cr alloy thin films

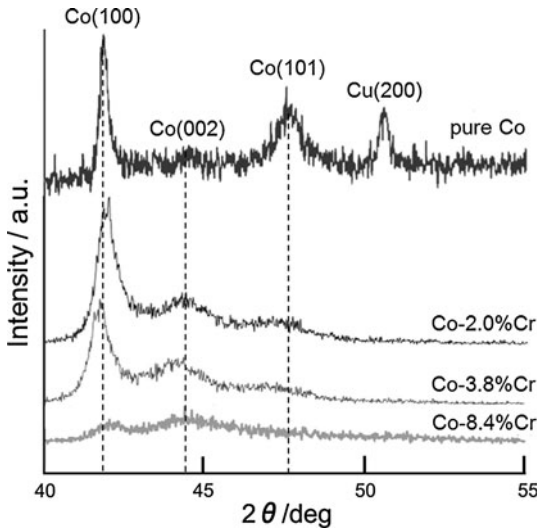

Fig. 5 X-ray diffraction profiles obtained from electrodeposited pure Co, Co—2.0 %Cr, Co—3.8 %Cr, and Co—8.4 %Cr alloy thin films

and γ' phase will be formed at the composition range more than 24 %Cr. On the contrary, according to the phase diagram of Co–Cr binary alloy system [20], the solubility limit of Cr in ε phase is ca. 14 % and σ phase will be formed at the composition range more than 57 %Cr. Hence, in the present work, it is suggested that the electrodeposited Ni—9.5 %Cr and Co—8.4 %Cr alloy forms a substitutional solid solution α phase and ε phase with fine crystals. Figure 6 shows SEM images of electrodeposited pure Ni (a), Ni—9.5 %Cr alloy (b), pure Co (c), and Co—8.4 %Cr alloy (d). The average crystal grains size of electrodeposited Ni—9.5 %Cr alloy (Fig. 6b) and Co—8.4 %Cr alloy (Fig. 6d) is a few micrometers, while that of pure Ni (Fig. 6a) and pure Co (Fig. 6c) is several tens nanometers. It was revealed that the average grains size of the electrodeposited alloys decreased with increase in R_{Cr}^{depo}.

Lin and Ho [21] reported that the Ni–Cr and Ni–Cr–P alloys with a fine-crystalline phase were electrodeposited from the solution containing dimethylformamide and methanol. They also found the Cr content in deposits decreased with increase in the bath temperature. Especially at elevated temperatures, dimethylformamide is hydrolyzed back into formic acid and dimethylamine in the presence of strong acid. Therefore, excess amount of formic ions will inhibit Cr^{3+} ions from electrodepositing. On the contrary, in the present work, the concentration of formic ions was fixed to 1.8 mol/L. Hence, effect of formic ions was kept to a stable condition to obtain the electrodeposited Ni–Cr and Co–Cr alloys. Li et al. [22] reported that Fe–Cr–P alloys with amorphous structure were electrodeposited from the aqueous solution containing glycine as a complexing agent. In their report, R_{Cr}^{depo} increased with increasing CCD. In the same way, 1.0 mol/L glycine was added to the electrolytic solutions as a complexing agent in the present work and R_{Cr}^{depo}

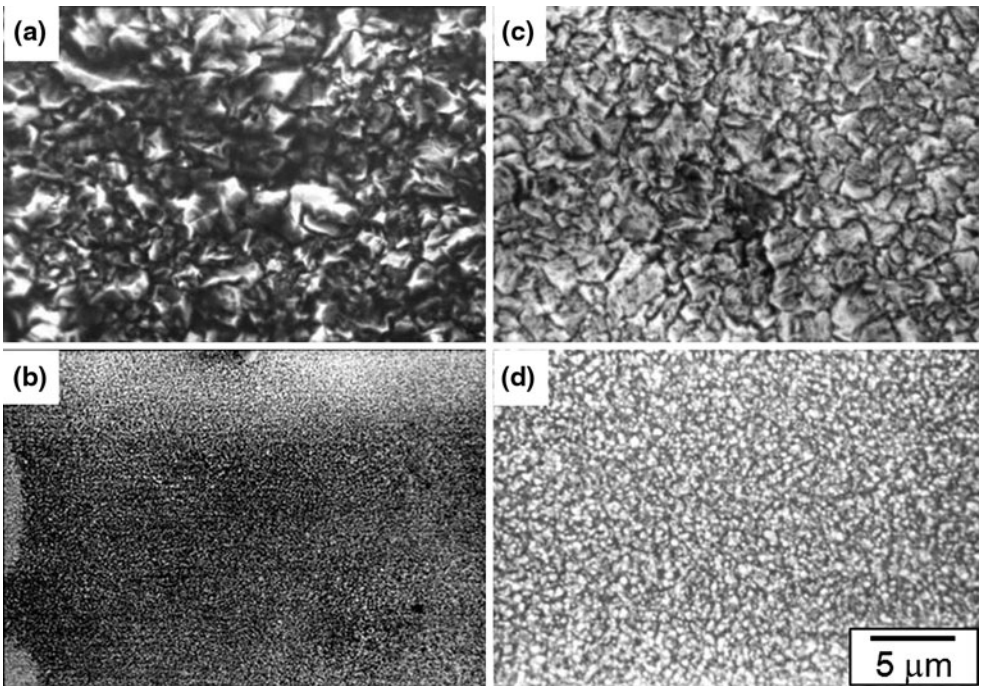

Fig. 6 SEM images of electrodeposited pure Ni (**a**), Ni—9.5 %Cr alloy (**b**), pure Co (**c**), and Co—8.4 %Cr alloy (**d**)

increased with increase in cathode potential as shown in Fig. 3. It is well known that the electrodeposition from stable complex ions accompanies with large over potential. Density of electrodeposited crystal nuclei on a cathode depends on the over potential. Usually, the density of nuclei increases with increasing the over potential up to a critical cathode potential region. However, if the cathode potential reaches a more negative region than the critical potential, diffusion limit of metal ions will occur and decomposition of water will proceed. In this excess over potential region, desirable metallic crystal nuclei will not be obtained. Electrodeposited fine-crystalline structure would be caused by the numerous fine-crystal nuclei. Therefore, in the present work, it is suggested that the fine-crystalline structure of electrodeposited Ni–Cr and Co–Cr alloy was introduced by an optimum over potential due to the reduction process from stable Cr^{3+} complex ions with glycine.

3.3 Magnetic properties of electrodeposited Ni–Cr and Co–Cr alloys

Magnetization curves of electrodeposited pure Ni (a), Ni—5.6 %Cr (b), Ni—9.5 %Cr (c), pure Co (d), Co—2.0 %Cr (e), and Co—8.4 %Cr (f) are shown in Fig. 7. Magnetic field was applied to inplane (dashed line) and perpendicular (solid line) direction to the film plane. Pure Ni and pure Co thin films were easily magnetized in in-plan direction and the magnetization reached to saturation at less than 1 kOe as shown in Fig. 7a, d. Coercive forces of the thin films were ca. 100 Oe. On the contrary, pure Ni and pure Co thin films were hardly magnetized in perpendicular direction. It is also well known that a crystalline magnetic thin film is hardly magnetized in perpendicular direction to the film plane due to the demagnetizing field caused by the inverse magnetic poles generated on the film surfaces [23]. The effective magnetic field, H_{eff}, can be expressed by the following equation:

$$H_{eff} = H_{\mathrm{a}} - H_{\mathrm{d}} = H_{\mathrm{a}} - f_{\mathrm{d}} M/\mu_0 \quad (3)$$

Here, H_{a} is the applied magnetic field, H_{d} is the demagnetizing field, f_{d} is the factor of demagnetizing field, M is magnetic moment, and μ_0 is permeability constant. When the magnetic field is applied to perpendicular direction to the film plane, f_{d} will be maximum value. In this case, H_{d} also becomes maximum value, hence H_{eff} will be minimum value and will not be enough to reach the saturation in magnetization. By the way, in the case of a thin film containing an array of nanowires with a large aspect more than ca. 100 [24–27], the array will be easily magnetized even in the perpendicular direction to the film plane due to decreasing f_{d}. On the contrary, when the magnetic field is applied to inplane direction to the film plane, f_{d} will be almost zero and H_{eff} will be equal to H_{a}. Therefore, pure Ni and pure Co thin films were easily magnetized in in-plan direction as shown in Fig. 6a, d.

As shown in Fig. 7c, f, the magnetizations of Ni—9.5 %Cr and Co—8.4 %Cr alloy reached to saturation at ca. 2.5 kOe even in perpendicular direction. Magnetic moment

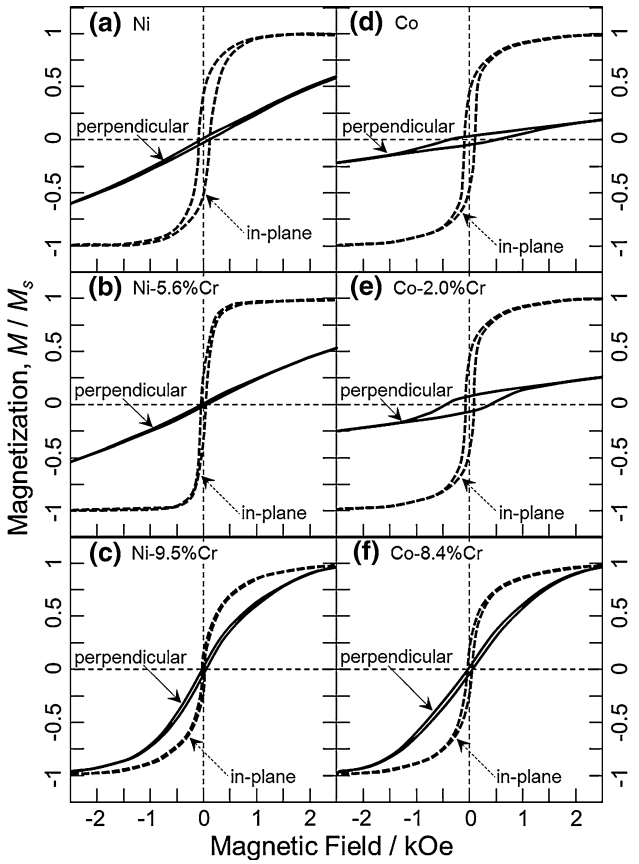

Fig. 7 Magnetization curves of electrodeposited pure Ni (**a**), Ni—5.6 %Cr (**b**), Ni—9.5 %Cr (**c**), pure Co (**d**), Co—2.0 %Cr (**e**), and Co—8.4 %Cr (**f**)

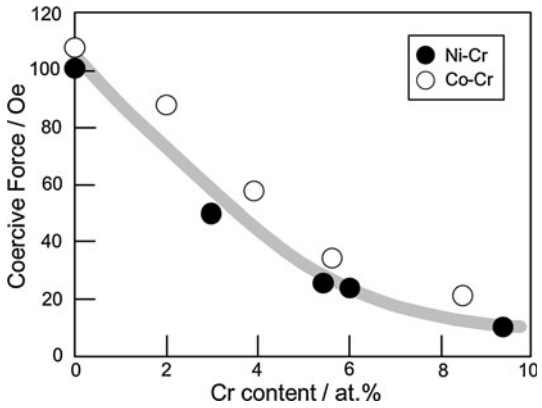

Fig. 8 Relationship between Cr contents in Ni–Cr or Co–Cr alloy deposits and the coercive force

M of Ni–Cr and Co–Cr alloy will decrease with increasing the content of non-magnetic Cr component. Kim et al. [28] also reported the magnetic moment M of Ni–Si alloy decreased with increasing the content of non-magnetic Si component. As shown in Eq. (3), demagnetizing field H_d is in proportion to the magnetic moment M which generates the inverse magnetic poles on the surfaces perpendicular to the magnetic field. On the other hand, Sulitanu [29] reported the structural origin of perpendicular magnetic anisotropy in electrodeposited Ni–W alloy thin films. According to his report, in the binary phase of nanocrystalline and amorphous, Ni–W alloy thin films with perpendicular magnetic anisotropy were obtained due to the characteristic structure with isolated columnar nanocrystalline grains surrounded by the amorphous phase. Furthermore, he suggested that the perpendicular magnetic anisotropy in Ni–W alloy thin films would be caused by the magnetoelastic anisotropy associated with inplane internal stresses and positive magnetostriction. Therefore, in the present work, it is estimated that the isotropical magnetization behaviors of Ni—9.5 %Cr and Co—8.4 %Cr alloys are caused by a columnar nanocrystalline phase and a magnetoelastic anisotropy induced from an inplane internal stress as well as increasing H_{eff} due to decreasing H_d in the perpendicular magnetic field direction to the film plane. Consequently, the magnetization behavior in perpendicular direction observed in the present work is resulted from increasing H_{eff} due to decreasing H_d in the perpendicular magnetic field direction to the film plane and the structure with nanocrystalline and amorphous phase.

Coercive forces of Ni—9.5 %Cr and Co—8.4 %Cr alloys were ca. 10 and 20 Oe, respectively, as shown in Fig. 7c, f; hence, the soft magnetic properties of electrodeposited Ni–Cr and Co–Cr alloys were improved with increase in R_{Cr}^{depo}. Relationship between R_{Cr}^{depo} and the coercive force H_c is shown in Fig. 8. With the increase in R_{Cr}^{depo}, H_c decreases hyperbolically. As shown in Fig. 6, the crystal grain size of Ni–Cr and Co–Cr alloys decreased with increase in R_{Cr}^{depo}. It is well known that H_c of ferromagnetic materials with nanocrystalline structure decreases with decreasing the crystal grain size [30]. Therefore, it is suggested that H_c of electrodeposited Ni–Cr and Co–Cr alloys decreased due to the decrease in crystal grain size of the deposits. However, excess Cr content in the alloy deposits will introduce the binary phase separation of a magnetic nanocrystalline phase and a non-magnetic Cr-rich phase [31]. According to the phase diagram of Ni–Cr and Co–Cr binary alloy system [20], in Ni–Cr alloy with R_{Cr}^{depo} more than ca. 20 % and Co–Cr alloy with R_{Cr}^{depo} more than ca. 15 %, the phase separation will occur at grain boundaries of the nanocrystalline phase. If the nanocrystalline grains are magnetically isolated with the non-magnetic Cr-rich precipitates, H_c of electrodeposited Ni–Cr and Co–Cr alloys will increase due to the formation of single magnetic domain structure which causes a magnetization reversal based on rotation process instead of domain wall motion.

4 Conclusions

With increase in cathode potential to less-noble direction, Cr content in the deposits also increased and Ni and Co

preferentially electrodeposited rather than Cr. Electrodeposition process of Ni–Cr and Co–Cr was categorized to "normal co-deposition type." Electrodeposited Ni—9.5 %Cr and Co—8.4 %Cr alloys formed a substitutional solid solution α phase and ε phase with fine crystals. Pure Ni and pure Co thin films were hardly magnetized in perpendicular direction to the film plane, while the magnetizations of Ni—9.5 %Cr and Co—8.4 %Cr alloy thin films reached to saturation at ca. 2.5 kOe even in perpendicular direction due to decreasing H_d with a decrease in M. H_c of electrodeposited Ni–Cr and Co–Cr alloys decreased due to a decrease in the crystal grain size of the deposits.

Acknowledgments This work was supported in part by the TDK Corporation, Mitutoyo Association for Science & Technology, Yazaki Memorial Foundation for Science & Technology, Research Foundation for Materials Science, Japan Society for the Promotion of Science (Grant-in-aid for Scientific Research C: No. 19560734).

References

1. Hoare JP (1979) On the mechanisms of chromium electrodeposition. J Electrochem Soc 126:190–199
2. Rosas WR, Robin A (2001) Cathodic film formation during chromium electrolysis on low-carbon steel using short duration current steps. J Appl Electrochem 31:531–536
3. Fontanesi C, Giovanardi R, Cannio M, Soragni E (2008) Chromium electrodeposition from Cr(VI) low concentration solutions. J Appl Electrochem 38:425–436
4. Drela I, Szynkarczuk J, Kubicki J (1989) Electrodeposition of chromium from Cr(III) electrolytes in the presence of formic acid. J Appl Electrochem 19:933–936
5. Giovanardi R, Orlando G (2011) Chromium electrodeposition from Cr(III) aqueous solutions. Surf Coat Technol 205:3947–3955
6. Kang JC, Lalvani SB, Melendres CA (1995) Electrodeposition and characterization of amorphous Fe–Ni–Cr-based alloys. J Appl Electrochem 25:376–383
7. Song YB, Chin DT (2002) Current efficiency and polarization behavior of trivalent chromium electrodeposition process. Electrochim Acta 48:349–356
8. Dolati AG, Ghorbani M, Afshar A (2003) The electrodeposition of quaternary Fe–Cr–Ni–Mo alloys from the chloride-complexing agents electrolyte. Part I. Processing. Surf Coat Technol 166:105–110
9. Protsenko V, Danilov F (2009) Kinetics and mechanism of chromium electrodeposition from formate and oxalate solutions of Cr(III) compounds. Electrochim Acta 54:5666–5672
10. McDougall J, El-Sharif M, Ma S (1998) Chromium electrodeposition using a chromium(III) glycine complex. J Appl Electrochem 28:929–934
11. Survilienė S, Nivinskienė O, Češunienė A, Selskis A (2006) Effect of Cr(III) solution chemistry on electrodeposition of chromium. J Appl Electrochem 36:649–654
12. Danilov FI, Protsenko VS, Gordiienko VO, Kwon SC, Lee JY, Kim M (2011) Nanocrystalline hard chromium electrodeposition from trivalent chromium bath containing carbamide and formic acid: structure, composition, electrochemical corrosion behavior, hardness and wear characteristics of deposits. Appl Surf Sci 257:8048–8053
13. Protsenko VS, Danilov FI, Gordiienko VO, Kwon SC, Kim M, Lee JY (2011) Electrodeposition of hard nanocrystalline chrome from aqueous sulfate trivalent chromium bath. Thin Solid Films 520:380–383
14. Howarth JN, Pletcher D (1988) The electrodeposition of chromium from chromium(III) solutions—a study using microelectrodes. J Appl Electrochem 18:644–652
15. Souza CAC, May JE, Machado AT, Tachard ALR, Bidoia ED (2005) Preparation of Fe–Cr–P–Co amorphous alloys by electrodeposition. Surf Coat Tech 190:75–82
16. Harris TM, Whitney GM, Croll IM (1995) The electrodeposition of Ni–Fe–Cr alloys for magnetic thin film applications. J Electrochem Soc 142:1031–1034
17. Stokłosa Z, Kwapuliński P, Rasek J, Badura G, Haneczok G, Pająk L, Lelątko L (2008) Structural relaxation, crystallization and improvement of magnetic properties in FeXSiB (X = Cr, Nb)-type amorphous alloys. J Magn Magn Mater 320:e762–e765
18. Bas JA, Calero JA, Dougan MJ (2003) Sintered soft magnetic materials: properties and applications. J Magn Magn Mater 254–255:391–398
19. Brenner A (1963) Electrodeposition of alloys. Academic Press, New York
20. Hansen M, Anderko K (1958) Constitution of binary alloys. McGraw-Hill, New York
21. Lin KL, Ho JK (1992) Electrodeposited Ni–Cr and Ni–Cr–P alloys. J Electrochem Soc 139:1305–1310
22. Li B, Lin A, Wu X, Zhang Y, Gan F (2008) Electrodeposition and characterization of Fe–Cr–P amorphous alloys from trivalent chromium sulfate electrolyte. J Alloys Compd 453:93–101
23. Pommier J, Meyer P, Penissard G, Ferre J, Bruno P, Renard D (1990) Magnetization reversal in ultrathin ferromagnetic films with perpendicular anisotropy: domain observations. Phys Rev Lett 65:2054–2057
24. Ohgai T, Enculescu I, Zet C, Westerberg L, Hjort K, Spohr R, Neumann R (2006) Magneto-sensitive nickel nanowires fabricated by electrodeposition into multi- and single-ion track templates. J Appl Electrochem 36:1157–1162
25. Ohgai T, Hjort K, Spohr R, Neumann R (2008) Electrodeposition of cobalt based ferro-magnetic metal nanowires in polycarbonate films with cylindrical nanochannels fabricated by heavy-ion-track etching. J Appl Electrochem 38:713–719
26. Spohr R, Zet C, Fischer BE, Kiesewetter H, Apel P, Gunko I, Ohgai T, Westerberg L (2010) Controlled fabrication of ion track nanowires and channels. Nucl Instrum Meth Phys Res B 268:676–686
27. Krimpalis S, Dragos OG, Moga AE, Lupu N, Chiriac H (2011) Magnetization processes in electrodeposited NiFe/Cu multilayered nanowires. J Mater Res 26:1081–1090
28. Kim DJ, Seol JK, Lee MR, Hyung JH, Kim GS, Ohgai T, Lee SK (2012) Ferromagnetic nickel silicide nanowires for isolating primary $CD4^+$ T lymphocytes. Appl Phys Lett 100:163703
29. Sulitanu N (2001) Structural origin of perpendicular magnetic anisotropy in Ni–W thin films. J Magn Magn Mater 231:85–93
30. Hernando A, Marin P, Vazquez M, Barandiaran JM, Herzer G (1998) Thermal dependence of coercivity in soft magnetic nanocrystals. Phys Rev B 58:366–370
31. Lodder JC (1996) Magnetic structures in Co–Cr media for perpendicular magnetic recording. J Magn Magn Mater 159:238–248